GRS 1739−278 OBSERVED AT VERY LOW LUMINOSITY WITH *XMM-Newton* AND *NuSTAR*

F. Fürst[1], J. A. Tomsick[2], K. Yamaoka[3,4], T. Dauser[5], J. M. Miller[6], M. Clavel[2], S. Corbel[7,8], A. Fabian[9], J. García[10], F. A. Harrison[1], A. Loh[7], P. Kaaret[11], E. Kalemci[12], S. Migliari[13,14], J. C. A. Miller-Jones[15], K. Pottschmidt[16,17], F. Rahoui[18,19], J. Rodriguez[7], D. Stern[20], M. Stuhlinger[13], D. J. Walton[20,1], and J. Wilms[5]

Draft version September 27, 2016

ABSTRACT

We present a detailed spectral analysis of *XMM-Newton* and *NuSTAR* observations of the accreting transient black hole GRS 1739−278 during a very faint low hard state at ∼0.02% of the Eddington luminosity (for a distance of 8.5 kpc and a mass of 10 $M_\odot$). The broad-band X-ray spectrum between 0.5–60 keV can be well-described by a power law continuum with an exponential cutoff. The continuum is unusually hard for such a low luminosity, with a photon index of $\Gamma = 1.39 \pm 0.04$. We find evidence for an additional reflection component from an optically thick accretion disk at the 98% likelihood level. The reflection fraction is low with $\mathcal{R}_{\rm refl} = 0.043^{+0.033}_{-0.023}$. In combination with measurements of the spin and inclination parameters made with *NuSTAR* during a brighter hard state by Miller and co-workers, we seek to constrain the accretion disk geometry. Depending on the assumed emissivity profile of the accretion disk, we find a truncation radius of 15–35 $R_{\rm g}$ (5–12 $R_{\rm ISCO}$) at the 90% confidence limit. These values depend strongly on the assumptions and we discuss possible systematic uncertainties.

Subject headings: stars: black holes — X-rays: binaries — X-rays: individual (GRS 1739-278) — accretion, accretion disks

1. INTRODUCTION

Galactic black hole (BH) transients typically undergo a very characteristic pattern during an outburst: during the first part of the rise, up to luminosities around 10% of the Eddington lu-

[1] Cahill Center for Astronomy and Astrophysics, California Institute of Technology, Pasadena, CA 91125, USA

[2] Space Sciences Laboratory, University of California, Berkeley, CA 94720, USA

[3] Solar-Terrestrial Environment Laboratory, Nagoya University, Furo-cho, Chikuka-ku, Nagoya, Aichi 464-8601, Japan

[4] Division of Particle and Astrophysical Science, Graduate School of Science, Nagoya University, Furo-cho, Chikuka-ku, Nagoya, Aichi 464-8602, Japan

[5] Dr. Karl-Remeis-Sternwarte and ECAP, Sternwartstr. 7, 96049 Bamberg, Germany

[6] Department of Astronomy, The University of Michigan, Ann Arbor, MI 48109, USA

[7] Laboratoire AIM (CEA/IRFU-CNRS/INSU-Université Paris Diderot), CEA DSM/IRFU/SAp, 91191 Gif-sur-Yvette, France

[8] Station de Radioastronomie de Nançay, Observatoire de Paris, PSL Research University, CNRS, Univ. Orléans, 18330 Nançay, France

[9] Institute of Astronomy, Madingley Road, Cambridge CB3 0HA, UK

[10] Harvard-Smithsonian Center for Astrophysics, Cambridge, MA 02138, USA

[11] Department of Physics and Astronomy, University of Iowa, Iowa City, IA 52242, USA

[12] Faculty of Engineering and Natural Sciences, Sabancı University, Orhanlı-Tuzla, 34956 Istanbul, Turkey

[13] European Space Astronomy Centre (ESAC), 28692 Villanueva de la Cañada, Madrid, Spain

[14] Department of Quantum Physics and Astrophysics & Institute of Cosmos Sciences, University of Barcelona, 08028 Barcelona, Spain

[15] International Centre for Radio Astronomy Research - Curtin University, GPO Box U1987, Perth, WA 6845, Australia

[16] CRESST, Department of Physics, and Center for Space Science and Technology, UMBC, Baltimore, MD 21250, USA

[17] NASA Goddard Space Flight Center, Greenbelt, MD 20771, USA

[18] European Southern Observatory, 85748 Garching bei Munchen, Germany

[19] Department of Astronomy, Harvard University, Cambridge, MA 02138, USA

[20] Jet Propulsion Laboratory, California Institute of Technology, Pasadena, CA 91109, USA

minosity ($L_{\rm Edd}$), they are in a so-called low/hard state. In this state the X-ray spectrum is dominated by a power law with a photon index Γ between ≈1.4–1.8 with almost no contribution from the thermal accretion disk spectrum. At higher Eddington rates the source switches to the high/soft state, where a steeper power law is observed and the thermal accretion disk dominates the soft X-ray spectrum (see, e.g., Remillard & McClintock 2006, for a description of BH states). Compelling evidence exists that in the soft state the accretion disk extends to the innermost stable circular orbit (ISCO), enabling spin measurements through relativistically smeared reflection features and thermal continuum measurements (e.g., Nowak et al. 2002; Miller et al. 2002; Steiner et al. 2010; McClintock et al. 2014; Petrucci et al. 2014; Kolehmainen et al. 2014; Miller et al. 2015; Parker et al. 2016).

At the end of an outburst the source transitions back to the low/hard state, albeit typically at much lower luminosities (≈1–4% $L_{\rm Edd}$) in a hysteretic behavior (see, e.g., Maccarone 2003; Kalemci et al. 2013). It has been postulated that the accretion disk recedes, i.e., the inner accretion disk radius $R_{\rm in}$ is no longer at the ISCO. Instead the inner regions are replaced by an advection dominated accretion flow (ADAF) in the inner few gravitational radii (e.g., Narayan & Yi 1995; Esin et al. 1997). Many observational results in a sample of different sources are at least qualitatively consistent with such a truncated disk as measured by, e.g., the frequency and width of quasi-periodic oscillations or multi-wavelength spectroscopy (see, e.g., Zdziarski et al. 1999; Esin et al. 2001; Kalemci et al. 2004; Tomsick et al. 2004).

It is still not clear, however, at what luminosity the truncation occurs and how it is triggered. There have been several reports of broad iron lines (implying a non-truncated disk) in the brighter part of the low/hard state (> 1% $L_{\rm Edd}$) for GX 339−4 (Miller et al. 2006; Reis et al. 2011; Allured et al. 2013) as well as for other systems (Reis et al. 2010; Reynolds et al. 2010), including GRS 1739−278 (Miller et al. 2015, hereafter M15).

Studies conducted recently mostly claim evidence for mod-

erate (tens of gravitational radii R_g) truncation at intermediate luminosities (≈ 0.5–10% L_Edd) in the low/hard state (Shidatsu et al. 2011; Allured et al. 2013; Petrucci et al. 2014; Plant et al. 2014). At a luminosity of $L = 0.14\%$ L_Edd in GX 339−4, Tomsick et al. (2009) measured a narrow Fe Kα line, indicating a significant truncation. While this suggests that gradual truncation may occur, it is not clear that R_in is only set by the luminosity (Petrucci et al. 2014; Kolehmainen et al. 2014; García et al. 2015). A more complex situation than a simple correlation with luminosity is also supported by recent measurements of the disk truncation at $\sim 10\,R_\mathrm{g}$ in GX 339−4 during intermediate states, i.e., during state transitions, at luminosities of 5–10% L_Edd (Tamura et al. 2012; Fürst et al. 2016a).

Besides the truncation radius, the geometry of the hot electron gas, or corona, is still unclear. It is very likely compact, and it has been postulated that it might be connected to the base of the jet, though a commonly accepted model has not yet emerged (see, e.g. Markoff et al. 2005; Reis & Miller 2013). *NuSTAR* and *Swift* observations of GX 339−4 in the low/hard state found that the reflector seems to see a different continuum than the observer, i.e., a hotter part of the corona (Fürst et al. 2015). This indicates a temperature gradient and a complex structure of the corona and seems to be independent of the spectral state (Parker et al. 2016).

It is clear from previous studies that the largest truncation radius is expected at the lowest luminosities, i.e., at the end and beginning of an outburst. High quality data in this state are traditionally difficult to obtain, given the low flux and necessary precise scheduling of the observations before the source vanishes into quiescence. With a combination of *XMM-Newton* (Jansen et al. 2001) and the *Nuclear Spectroscopy Telescope Array* (*NuSTAR*, Harrison et al. 2013), however, such observations are now possible.

Here we report on *XMM-Newton* and *NuSTAR* observations of the BH transient GRS 1739−278 in the declining phase of its very long outburst in 2014/2015 (Figure 1). GRS 1739−278 is a transient BH candidate, discovered by *Granat* (Paul et al. 1996; Vargas et al. 1997). It is most likely located close to the Galactic Center at a distance of ≈ 8.5 kpc. The large extinction ($A_V = 14 \pm 2$, Greiner et al. 1996) makes a spectral identification of the companion difficult, but from photometric data, Marti et al. (1997) and Chaty et al. (2002) infer a late-type main-sequence star of at least F5 V or later.

GRS 1739−278 was classified as a BH candidate given its similarity in spectral evolution to other transient BHs as well as the presence of a very strong 5 Hz QPO in the soft-intermediate state (Borozdin et al. 1998; Borozdin & Trudolyubov 2000).

During the beginning of the 2014/2015 outburst, *NuSTAR* measured a strong reflection spectrum and a relativistically broadened iron line in a bright low/hard state (M15). These authors could constrain the size of the corona, assuming a lamppost model, to be $< 22\,R_\mathrm{g}$ and the truncation radius to $R_\mathrm{in} = 5^{+3}_{-4}\,R_\mathrm{g}$. In the lamppost geometry the corona is assumed to be a point-like source located on the spin axis of the BH and shining down onto the accretion disk (Matt et al. 1991; Dauser et al. 2013). The luminosity during this observation was around $8\%L_\mathrm{Edd}$ (assuming a canonical mass of $10\,\mathrm{M}_\odot$), at which no truncation of the accretion disk is expected.

After the first *NuSTAR* observation, the source continued with a typical outburst evolution and faded to very low luminosities around MJD 57000. However, it probably never reached quiescent levels and *Swift*/XRT and BAT monitoring
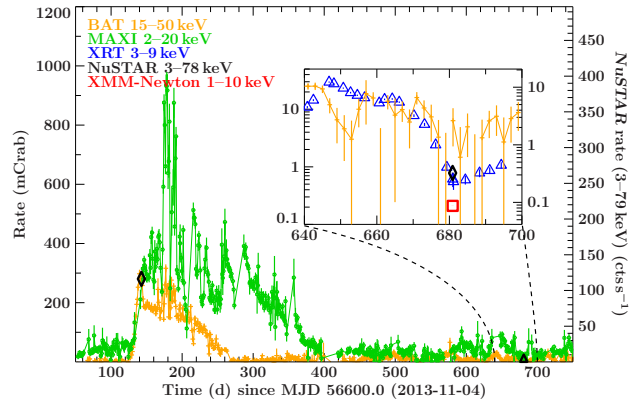

FIG. 1.— *Swift*/BAT (15–50 keV, orange; Krimm et al. 2013) and MAXI/GSC (2–20 keV, green; Matsuoka et al. 2009) monitoring light curve of GRS 1739−278. The *NuSTAR* observations (3–79 keV) are marked by black diamonds, the one presented by Miller et al. (2015) occurred around 150 d, the one presented here around 680 d. All data are shown in observed (i.e., absorbed) count-rates rescaled to mCrab fluxes in the respective energy band of the instrument. The right-hand y-axis gives the average measured *NuSTAR* count-rate of the observation. The inset shows a zoom-in on the 2015 data, including *Swift*/XRT (Burrows et al. 2005) data (3–9 keV, blue triangles) and the *XMM-Newton* observation (1–10 keV, red square). Due to the crowded source region the MAXI data suffer from increased background of about 40 mCrab and are therefore not shown in the inset. Note that the inset y-axes are scaled logarithmically.

indicated that it also did not switch back to a stable low/hard state. A detailed description of the evolution will be presented by Loh et al. (in prep.). Around MJD 57272 the monitoring data indicated a stable transition to the low/hard state had occurred, confirmed by a brightening in the radio. We then triggered simultaneous *XMM-Newton* and *NuSTAR* observations to observe a very faint hard state, and found GRS 1739−278 at ~0.02% L_Edd.

The rest of the letter is structured as follows: in Section 2 we describe the data reduction and calibration. In Section 3 we present the spectral analysis and compare it to results by M15. In the last section, Section 4, we discuss our results and put them into context.

2. DATA REDUCTION AND OBSERVATION

2.1. *NuSTAR*

NuSTAR observed GRS 1739−278 on MJD 57281 (ObsID 80101050002) for a good exposure time, after standard screening, of 43 ks per module. We extracted the *NuSTAR* data using HEASOFT v6.15 and the standard `nupipeline` v1.4.1 from a 50″ region centered on the J2000 coordinates of GRS 1739−278. On both focal plane modules (FPMs) the source was located in an area of enhanced background due to stray-light from sources outside the field-of-view, dominated by GX 3+1. We tested different background regions and found that the exact choice only marginally influences the source spectrum. We obtained good agreement between FPMA and FPMB. Despite the high background level we obtained a detection up to 60 keV. We used *NuSTAR* data between 3–60 keV and rebinned them to a signal-to-noise ratio (S/N) of 6 per bin and at least 2 channels per bin (Figure 2a).

2.2. *XMM-Newton*

We obtained simultaneous *XMM-Newton* observations with a good exposure time of 79 ks in EPIC-pn (Strüder et al. 2001), using the timing mode (ObsID 0762210201). *XMM-Newton* data were extracted using SAS v14.0.0. The source spectrum was extracted from columns RAWX 33–42 and the

background from columns RAWX 50–60 using only single and double events (PATTERN 0–4). The first 15 ks of the observation were strongly contaminated by background flares, and we excluded these data. The background continued to be elevated throughout the whole observation, in particular influencing the spectrum below 1 keV. In the remainder of the paper, we therefore use EPIC-pn data between 0.6–10 keV, rebinned to a S/N of 5 with at least 5 channels per bin.

We also obtained EPIC-MOS (Turner et al. 2001) data in timing mode. Due to a hot column, calibration of the MOS 1 timing mode is difficult and we therefore ignore these data. For the MOS 2 data, the source spectrum was extracted from columns RAWX 294–314 and the background from columns RAWX 260–275 using only single events (PATTERN=0) with FLAG=0. MOS 2 data add up to a good exposure time of 35 ks and were rebinned to a S/N of 5 with at least 3 channels per bin between 0.7–10 keV. They agree very well with the EPIC-pn data (Figure 2).

3. SPECTRAL ANALYSIS

Using the Interactive Spectral Interpretation System (ISIS v1.6.2, Houck & Denicola 2000) we fit the *XMM-Newton* and *NuSTAR* spectra simultaneously. Uncertainties are reported at the 90% confidence level unless otherwise noted. We allowed for a cross-calibration constant (CC) between the instruments to take differences in absolute flux calibration into account. All fluxes are given with respect to *NuSTAR*/FPMA. The other instruments are within a few percent of these values, besides MOS 2, which measures fluxes up to 15% lower. This discrepancy is within the expected uncertainty of the MOS timing mode.

We model the absorption using an updated version of the `tbabs`[21] model and its corresponding abundance vector as described by Wilms et al. (2000) and cross-sections by Verner et al. (1996). As found by M15 and other previous works, the column density is around 2×10^{22} cm^{-2}, in agreement with the estimates from the dust scattering halo found around GRS 1739−278 (Greiner et al. 1996).

Using an absorbed power law continuum with an exponential cutoff provides a statistically acceptable fit, with $\chi^2_{\rm red} = 1.08$ ($\chi^2 = 1023$) for 946 degrees of freedom (d.o.f.). The best-fit values are given in Table 1 and the residuals are shown in Figure 2b. Small deviations around 1 keV can be attributed to known calibration uncertainties in the EPIC instruments.

Compared to the earlier observation discussed by M15, the spectrum of the later observation discussed here is significantly harder, with a lower photon index Γ and a higher folding energy $E_{\rm fold}$ (labeled $E_{\rm cut}$ in the `cutoffpl` model and in M15). This is not only true when compared to the simple cutoff power law model of M15, which does not provide an adequate fit to their data, but also when compared to the underlying continuum when adding an additional reflection component (see Table 1 in M15).

The `cutoffpl` is continuously curving (even far below the folding energy) and does not necessarily accurately describe a Comptonization spectrum (Fürst et al. 2016b; Fabian et al. 2015). We therefore also tested the Comptonization model `nthcomp` (Zdziarski et al. 1996; Życki et al. 1999) and find a comparable fit with $\chi^2_{\rm red} = 1.08$ ($\chi^2 = 1022$) for 945 d.o.f. (Table 1). We find a plasma temperature of $kT_{\rm e} = 15.5^{+6.3}_{-2.7}$ keV, which, when multiplied with the expected
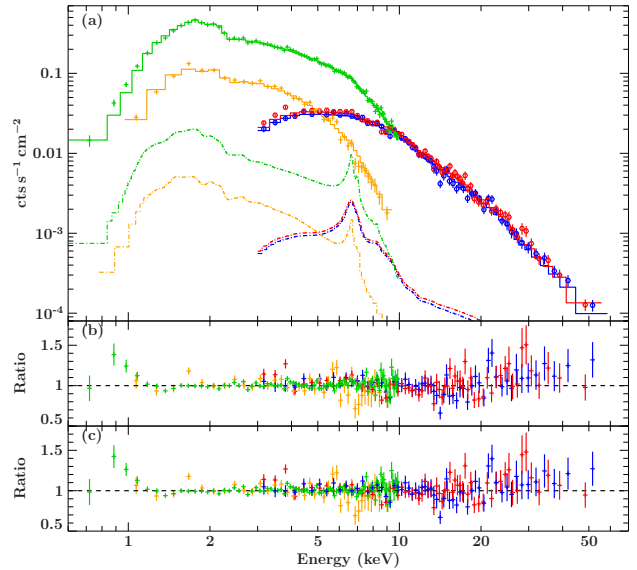
FIG. 2.— *(a)* Data and best-fit `xillver` model. *XMM-Newton*/EPIC-pn is shown in green, MOS 2 in orange, *NuSTAR*/FPMA in red and FPMB in blue. The dashed lines show the contribution of the reflection in each instrument. *(b)* Residuals to the cutoff-power law model. *(c)* Residuals to the reflection (`xillver`) model. Data were rebinned for visual clarity.

factor of 3, agrees well with the measured folding energy of the `cutoffpl`.

We next search for signatures of reflection, which is present in all low/hard state spectra of accreting black holes, even at low luminosities (see, e.g., Tomsick et al. 2009; Fürst et al. 2015). To model the reflection we use the `xillver` model v0.4a (García & Kallman 2010; García et al. 2013), which self-consistently describes the iron line and Compton hump. The model is based on a cutoff power law as the input continuum and we therefore also use the cutoff power law to describe the continuum spectrum.

With this model we find a statistically good fit with $\chi^2_{\rm red} = 1.06$ ($\chi^2 = 1005$) for 943 d.o.f. We show this model with the data and the contribution of the reflection in Figure 2a and its residuals in Figure 2c. This is an improvement of $\Delta\chi^2 = 15$ for 3 fewer degrees of freedom. According to the sample-corrected Akaike Information Criterion (AIC, Akaike 1974), this is a significant improvement of ΔAIC=8.8, i.e., at >98% likelihood (Burnham et al. 2011).

We find a low, but well constrained reflection fraction of $\mathcal{R}_{\rm refl} = 0.045^{+0.044}_{-0.022}$ and a high ionization parameter of $\log(\xi/({\rm erg\,cm\,s}^{-1})) = 3.22^{+0.43}_{-0.27}$. The iron abundance $A_{\rm Fe}$ is not well constrained but seems to prefer values > 2.5 solar, relative to the solar abundances by Grevesse & Sauval (1998), on which the `xillver` model is based (Table 1). Fixing the iron abundance to 1 times solar results in a slightly worse fit with $\chi^2_{\rm red} = 1.07$ ($\chi^2 = 1013$) for 944 d.o.f., but none of the other parameters changes significantly. We cannot constrain the ratio between neutral and ionized iron due to small contribution of the reflection component to the overall spectrum.

While the phenomenological models presented above provide a statistically very good fit, they do not contain information about the geometry of the X-ray producing region. To obtain information about the geometry we need to study the strong relativistic effects close to the BH, in particular the relativistic broadening of the reflection features. These features have been used by M15 in the bright hard state data to measure the spin of the BH in GRS 1739−278 to be $a = 0.8 \pm 0.2$

TABLE 1
BEST-FIT MODEL PARAMETERS.

Parameter	Cutoffpl	Nthcomp	Xillver	Relxill	Relxilllp
N_{H} (10^{22} cm^{-2})	2.13 ± 0.05	1.44 ± 0.06	$2.17^{+0.07}_{-0.05}$	$2.16^{+0.06}_{-0.05}$	$2.16^{+0.06}_{-0.05}$
$\mathcal{F}$ (10^{-11} erg cm^{-2} s^{-1})[a]	2.89 ± 0.06	2.79 ± 0.05	$2.90^{+0.07}_{-0.04}$	2.91 ± 0.06	2.91 ± 0.06
Γ	1.40 ± 0.04	$1.637^{+0.016}_{-0.014}$	$1.409^{+0.038}_{-0.026}$	$1.404^{+0.030}_{-0.031}$	$1.404^{+0.030}_{-0.031}$
E_{fold}/kT (keV)	56^{+15}_{-10}	$15.5^{+6.3}_{-2.7}$	61^{+20}_{-10}	58^{+14}_{-10}	58^{+14}_{-10}
A_{Fe}	—	—	$5.0^{+5.1}_{-2.5}$	1.5^{c}	1.5^{c}
$\log \xi$ (erg cm s^{-1})	—	—	$3.22^{+0.43}_{-0.27}$	$3.22^{+0.23}_{-0.46}$	$3.24^{+0.22}_{-0.49}$
$\mathcal{R}_{\mathrm{refl}}$	—	—	$0.045^{+0.044}_{-0.022}$	$0.08^{+0.06}_{-0.05}$	0.099^{b}
i	—	—	$32.5^{\circ\mathrm{c}}$	$32.5^{\circ\mathrm{c}}$	$32.5^{\circ\mathrm{c}}$
R_{in} (R_{g})	—	—	—	> 15	> 35
R_{out} (R_{g})	—	—	—	400^{c}	400^{c}
H (R_{g})	—	—	—	—	30^{+100}_{-27}
q	—	—	—	3^{c}	—
a	—	—	—	0.8^{c}	0.8^{c}
CC_B	$0.979^{+0.025}_{-0.024}$	$0.979^{+0.025}_{-0.024}$	$0.984^{+0.022}_{-0.029}$	$0.980^{+0.025}_{-0.024}$	$0.980^{+0.025}_{-0.024}$
CC_{pn}	$0.960^{+0.020}_{-0.019}$	0.949 ± 0.020	$0.958^{+0.015}_{-0.026}$	0.954 ± 0.020	0.954 ± 0.020
CC_{MOS}	$0.884^{+0.024}_{-0.023}$	$0.872^{+0.024}_{-0.023}$	$0.884^{+0.020}_{-0.029}$	$0.880^{+0.024}_{-0.023}$	$0.880^{+0.024}_{-0.023}$
χ^2/d.o.f.	1022.70/946	1022.48/945	1005.78/943	1012.06/943	1012.31/943
χ^2_{red}	1.081	1.082	1.067	1.073	1.073

[a] between 1–30 keV

and constrain the radius of the inner accretion disk to be close to the ISCO.

Due to the low count rates and low reflection strength, our data do not allow us to constrain all parameters of the relativistic smearing models. We therefore fix values that are unlikely to change on time-scales of the outburst, namely the inclination i and the iron abundance A_{Fe}, to the values found by M15 for the `relxilllp` model: $i = 32.5°$ and $A_{\mathrm{Fe}} = 1.5$. We fix the spin to $a = 0.8$, the best-fit value of the `relxill` model by M15, as it was unconstrained in their lamppost geometry (`relxilllp`) model. By fixing the inclination, we ignore possible effects of a warped disk.

We model the relativistic effects using the `relxill` model (Dauser et al. 2013; García et al. 2014) with the emissivity described by a power law with an index of 3, which is appropriate for a standard Shakura-Sunyaev accretion disk and an extended corona (Dabrowski et al. 1997). We also set the outer disk radius to $r_{\mathrm{out}} = 400\,R_{\mathrm{g}}$. This model gives a good fit with $\chi^2_{\mathrm{red}} = 1.07$ ($\chi^2 = 1012$) for 943 d.o.f., and its best-fit parameters are shown in Table 1. This fit is statistically slightly worse compared to the `xillver` model, but presents the more physically realistic description of the spectrum. The main driver of reduced statistical quality is the iron abundance, which we held fixed. If we allow it to vary, we find a fit with $\chi^2_{\mathrm{red}} = 1.07$ ($\chi^2 = 1332$) for 1246 d.o.f., i.e., the same as for the `xillver` model. However, as in the `xillver` model, the iron abundance is only weakly constrained and the other parameters do not change significantly. Thus, we keep it fixed at the better constrained value from M15 for the remainder of this work. We only obtain a lower limit on the inner accretion disk radius, $R_{\mathrm{in}} > 15\,R_{\mathrm{g}}$.

Allowing for a variable emissivity index does not improve the fit significantly and results in a similar constraint for the inner radius ($R_{\mathrm{in}} > 15\,R_{\mathrm{g}}$). The emissivity index itself is not constrained between $3 \leq q \leq 10$. The often used broken power law emissivity profile can therefore not be constrained either, in particular because the expected break radius is smaller than the inner accretion disk radius we find (see M15, and references therein).

For the most self-consistent description of the reflection and relativistic blurring we use the `relxilllp` model, i.e., assum-

ing a lamppost geometry for the corona. While this is a simplified geometry in which the corona is assumed to be a point source on the spin axis at a given height H above the BH (see, e.g., Dauser et al. 2013), it is the only geometry where the reflection fraction can be calculated self-consistently based on ray-tracing calculations.[22]

This model also gives an acceptable fit with $\chi^2_{\mathrm{red}} = 1.07$ ($\chi^2 = 1012$) for 943 d.o.f.; see Table 1. Compared to the previous model, the reflection fraction is now expressed in terms of coronal height. We obtain a lower limit for the inner radius $R_{\mathrm{in}} > 35\,R_{\mathrm{g}}$, while the coronal height H is completely unconstrained over the allowed range of 3–100 R_{g} (where the lower limit is set by the ISCO for a BH with spin $a = 0.8$ and the upper limit is determined to be at a height where changes in H only influence the model marginally).

As both H and R_{in} are directly related to the reflection fraction, and the reflection fraction is relatively well-constrained, as shown in the `relxill` model, we expect a strong degeneracy between these parameters. We therefore calculate a confidence contour between them, shown in Figure 3. While this confirms the degeneracy between these two parameters, an inner radius $< 17.5\,R_{\mathrm{g}}$ is ruled out at the 99% confidence level for all values of H.

As the reflection fraction is taken into account self-consistently in this model, we can calculate it based on the values for H and R_{in} (and a and r_{out} which have been held fixed). Similar values for the reflection can be achieved over a wide range of values for H and R_{in}, as shown by the color-coded map in the background of Figure 3. The confidence contours follow areas of constant reflection fraction closely.

4. DISCUSSION AND CONCLUSION

We have presented a spectral analysis of *XMM-Newton* and *NuSTAR* observations of GRS 1739−278 during a very faint hard state. The luminosity between 1–80 keV was about 3×10^{35} erg s^{-1}, i.e., only about 0.02% of the Eddington luminosity for a prototypical $10\,\mathrm{M}_\odot$ BH at a distance of 8.5 kpc.

---

[22] In principle the reflection fraction can be calculated in this way for any geometry (see, e.g., Wilkins & Fabian 2012), but such calculations are too computationally intensive to be performed while fitting astrophysical data
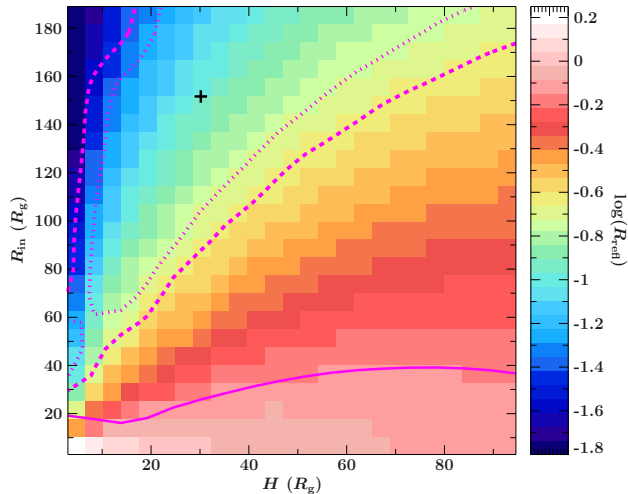
FIG. 3.— Confidence contours of χ^2 for the self-consistent `relxilllp` model as a function of coronal height H and inner radius R_{in}. The lines indicate the 1σ (dotted), 90% (dashed) and 99% (solid) confidence levels for two parameters of interest. The 99% level only provides a lower limit to the inner radius. The cross marks the best-fit value. The color-coded map in the background shows the corresponding reflection fraction according to the scale on the right.

The *XMM-Newton* and *NuSTAR* spectra agree very well and provide, despite the low source flux, a high-quality spectrum between 0.5–60 keV. While the reflection features are weak, they are still detected at > 98% confidence in our data.

The spectrum is very hard with a photon index around 1.4 and a folding energy at ∼60 keV. It is somewhat surprising to find such a hard spectrum at the very low Eddington luminosity observed. Typically the photon index decreases with decreasing flux only down to a transitional luminosity of ∼1% L_{Edd}, after which the photon index begins to increase again with lower luminosities (see, e.g., Tomsick et al. 2001; Wu & Gu 2008; Yang et al. 2015). During quiescence the photon index has been seen to increase to $\Gamma \geq 2$ (Corbel et al. 2006; Plotkin et al. 2013). The lowest photon-indices at the transitional luminosity are typically ∼ 1.5 (Kalemci et al. 2013; Wu & Gu 2008).

We observe a harder photon index at roughly two orders of magnitude below the typically expected transition luminosity. Our inferred Eddington luminosity depends on the assumption of mass and distance, but even with their large uncertainties, it is difficult to increase the luminosity by two orders of magnitude. In any case, the measured hard photon index is at the lower end of known indices and comparable to the hardest spectrum found by Belloni et al. (2002) for XTE J1550−564. This may indicate that thermal Comptonization in an optically thin plasma is still the dominating effect in GRS 1739−278, even though a strong radio jet is present (e.g., Loh et al., in prep.), as a jet-dominated synchrotron spectrum would result in a softer photon index (Esin et al. 1997; Yang et al. 2015).

A faint hard state of the prototypical transient BH binary GX 339−4 was presented by Fürst et al. (2015), at an estimated luminosity of 0.94% L_{Edd}. We found that the spectrum incident on the reflector was harder than the observed continuum, with a best-fit photon index of $\Gamma = 1.31^{+0.01}_{-0.31}$. This is similar to the values we measure for GRS 1739−278. Fürst et al. (2015) argue that the inner parts of the corona, which are preferentially intercepted and reprocessed by the accretion disk, might be hotter than parts farther away from the BH, which are more likely to be visible by a distant observer.

If in GRS 1739−278 the accretion disk is truncated or its inner parts are optically thin, we would have a direct line of sight towards the hot inner parts of the corona, explaining the observed hard power law.

In GRS 1739−278 we find a relatively low folding energy of ∼60 keV. In the `nthcomp` Comptonization model we find a corresponding low electron temperature around 16 keV (resulting in a high optical depth of $\tau > 3$, Sunyaev & Titarchuk 1980). Such a cool corona is unusual at these low luminosities (Tomsick et al. 2001; Miyakawa et al. 2008; Fürst et al. 2015). However, there are a few examples of other BH systems that have shown a low cutoff energy together with a hard photon index (e.g., GRO J1655−40, Kalemci et al. 2016). We note that M15 also found a relatively low cutoff energy of 28 keV, cooler than in our observation. It is therefore possible that GRS 1739−278 has a generally cooler corona than comparable BH binaries.

We applied two relativistic reflection models to the GRS 1739−278 data, with different assumptions: either assuming a constant emissivity index of $q = 3$ or a self-consistent emissivity and reflection fraction in the lamppost geometry. In both cases we find a significantly truncated accretion disk at the 90% confidence limit at $R_{in} > 15\,R_g$ and > 35 R_g, respectively. In the self-consistent lamppost model, we can even rule out an accretion disk with an inner radius $\lesssim 20\,R_g$ at the 99% level. However, all these values are strongly dependent on our assumptions. In the following we will discuss three assumptions influencing the systematic uncertainties.

The coronal and disk geometry: While the lamppost geometry is likely a significant simplification of the real geometry (e.g., by assuming a point-like corona), there are strong indications that the X-ray corona is compact, at least at luminosities $L \gtrsim 1\% L_{Edd}$ (e.g., Reis & Miller 2013). Furthermore, when describing the emissivity with a broken power law, values resembling the lamppost geometry of a corona close to the black hole, i.e., a very steep inner index and a much flatter outer index, are often found (e.g., Wilkins & Fabian 2012, M15). However, the coronal structure in the very low hard state, as observed here, is much less certain, and the applicability of a lamppost corona is unclear. For example, if most parts of the inner accretion disk are replaced by an ADAF, the ADAF itself could act as the Compton upscattering hot electron gas. In this case the inner accretion disk would naturally be truncated as well.

We note that the non-relativistic `xillver` model provides a good fit to the data and that the relativistic models are consistent with a neutral ionization parameter. This could indicate that the reflection occurs very far away from the BH, maybe in neutral material independent of the accretion disk or possibly on the companion's surface. This would be possible for strongly beamed and misaligned coronal emission and is also consistent with a strongly truncated accretion disk.

It is possible that the corona is outflowing and thereby beaming most of its radiation away from the accretion disk. In this case, we would observe a low reflection fraction despite a non-truncated accretion disk (Beloborodov 1999). This model is particularly relevant if the corona is associated with the base of a relativistic jet, which is known to be present due to the strong flux in the radio (Loh et al., in prep.). However, the data quality does not allow us to constrain such an outflow and we can therefore not quantitatively assess this possibility.

Inclination: Here we assume an inclination of 32.5°, as found by M15 for the lamppost geometry. In the model pre-

ferred by M15, with an emissivity described by a broken power law, they find 43.2° instead. When using this higher inclination, we find a truncated accretion disk at $> 28\,R_{\rm g}$ at the 90% level, and we can no longer constrain the radius at the 99% level, even with the self-consistent lamppost model (i.e., all inner radii between 3–200 $R_{\rm g}$ are allowed at the 99% level). It is possible that the inclination of the accretion disk changed between the two observations, e.g., due to a warped disk (e.g., Tomsick et al. 2014), so that a large range of values is possible. Our data do not allow us to constrain the disk inclination independently.

Outer radius: as we find that our data are consistent with large values of the inner truncation radius ($R_{\rm in} \geq 200\,R_{\rm g}$), we investigate if the choice of the outer accretion disk radius influences the constraints. As the reflection fraction is calculated self-consistently from the size of the accretion disk in the `relxilllp` model, a change in outer radius will influence the inferred reflection fraction. The typical assumption in most relativistic reflection models is an outer radius of $400\,R_{\rm g}$, which is justified for steep emissivity indices. To confirm that this choice does not influence our measurement, we stepped the outer radius from $400\,R_{\rm g}$ to $1000\,R_{\rm g}$ (the upper limit of the `relxilllp` model) and find consistent values of $R_{\rm in} \approx 20\,R_{\rm g}$ at the 99% limit.

Another important parameter for relativistic reflection models is the BH spin, a, which we held fix at 0.8 as found by M15. While this value is not well constrained, changes of the spin do not influence the spectral fits in our case, given the large inner radius we find. Even for a non-spinning BH our lower limits are far outside the ISCO, which would be at $6\,R_{\rm g}$. The exact value of the spin parameters therefore does not change our conclusions.

In conclusion we have shown that the combination of *XMM-Newton* and *NuSTAR* allows us to get a more detailed look at BH accretion at lower Eddington luminosities than ever before. We can constrain the underlying continuum very well and find strong indications that the accretion disk is truncated at a minimum of $15\,R_{\rm g}$, i.e., $\sim 5\,R_{\rm ISCO}$ for a BH with spin $a = 0.8$. However, even with these data, a unique deter-mination of the geometry of the corona and the accretion disk in this state cannot be found due to the lack of photons as well as strong degeneracies in the models.

Facilities: NuSTAR, XMM

REFERENCES

Akaike H., 1974, IEEE Transactions on Automatic Control 19, 716
Allured R., Tomsick J.A., Kaaret P., Yamaoka K., 2013, ApJ 774, 135
Belloni T., Colombo A.P., Homan J., et al., 2002, A&A 390, 199
Beloborodov A.M., 1999, ApJ 510, L123
Borozdin K.N., Revnivtsev M.G., Trudolyubov S.P., et al., 1998, Astron. Let. 24, 435
Borozdin K.N., Trudolyubov S.P., 2000, ApJL 533, L131
Burnham K.P., Anderson D.R., Huyvaert K.P., 2011, Behav. Ecol. Sociobiol 65, 23
Burrows D.N., Hill J.E., Nousek J.A., et al., 2005, SSRv 120, 165
Chaty S., Mirabel I.F., Goldoni P., et al., 2002, MNRAS 331, 1065
Corbel S., Tomsick J.A., Kaaret P., 2006, ApJ 636, 971
Dabrowski Y., Fabian A.C., Iwasawa K., et al., 1997, MNRAS 288, L11
Dauser T., García J., Wilms J., et al., 2013, MNRAS 430, 1694
Esin A.A., McClintock J.E., Drake J., et al., 2001, ApJ 555, 483
Esin A.A., McClintock J.E., Narayan R., 1997, ApJ 489, 865
Fabian A.C., Lohfink A., Kara E., et al., 2015, MNRAS 451, 4375
Fürst F., Grinberg V., Tomsick J.A., et al., 2016a, ApJ 828, 34
Fürst F., Müller C., Madsen K.K., et al., 2016b, ApJ 819, 150
Fürst F., Nowak M.A., Tomsick J.A., et al., 2015, ApJ 808, 122
García J., Dauser T., Lohfink A., et al., 2014, ApJ 782, 76
García J., Dauser T., Reynolds C.S., et al., 2013, ApJ 768, 146
García J., Kallman T.R., 2010, ApJ 718, 695
García J.A., Steiner J.F., McClintock J.E., et al., 2015, ApJ 813, 84
Greiner J., Dennerl K., Predehl P., 1996, A&A 314, L21
Grevesse N., Sauval A.J., 1998, SSRv 85, 161

Harrison F.A., Craig W., Christensen F., et al., 2013, ApJ 770, 103
Houck J.C., Denicola L.A., 2000, In: Manset N., Veillet C., Crabtree D. (eds.) Astronomical Data Analysis Software and Systems IX, Vol. 216. Astronomical Society of the Pacific Conference Series, Astron. Soc. Pac., San Francisco, p. 591
Jansen F., Lumb D., Altieri B., et al., 2001, A&A 365, 6
Kalemci E., Begelman M.C., Maccarone T.J., et al., 2016, MNRAS 463, 615
Kalemci E., Dinçer T., Tomsick J.A., et al., 2013, ApJ 779, 95
Kalemci E., Tomsick J.A., Rothschild R.E., et al., 2004, ApJ 603, 231
Kolehmainen M., Done C., Díaz Trigo M., 2014, MNRAS 437, 316
Krimm H.A., Holland S.T., Corbet R.H.D., et al., 2013, ApJS 209, 14
Maccarone T.J., 2003, A&A 409, 697
Markoff S., Nowak M.A., Wilms J., 2005, ApJ 635, 1203
Marti J., Mirabel I.F., Duc P.A., Rodriguez L.F., 1997, A&A 323, 158
Matsuoka M., Kawasaki K., Ueno S., et al., 2009, PASJ 61, 999
Matt G., Perola G.C., Piro L., 1991, A&A 247, 25
McClintock J.E., Narayan R., Steiner J.F., 2014, SSRv 183, 295
Miller J.M., Fabian A.C., Wijnands R., et al., 2002, ApJL 570, L69
Miller J.M., Homan J., Steeghs D., et al., 2006, ApJ 653, 525
Miller J.M., Tomsick J.A., Bachetti M., et al., 2015, ApJL 799, L6 (M15)
Miyakawa T., Yamaoka K., Homan J., et al., 2008, PASJ 60, 637
Narayan R., Yi I., 1995, ApJ 452, 710
Nowak M.A., Wilms J., Dove J.B., 2002, MNRAS 332, 856
Parker M.L., Tomsick J.A., Kennea J.A., et al., 2016, ApJL 821, L6
Paul J., Bouchet L., Churazov E., Sunyaev R., 1996, IAUC 6348
Petrucci P.O., Cabanac C., Corbel S., et al., 2014, A&A 564, A37

Plant D.S., Fender R.P., Ponti G., et al., 2014, MNRAS 442, 1767
Plotkin R.M., Gallo E., Jonker P.G., 2013, ApJ 773, 59
Reis R.C., Fabian A.C., Miller J.M., 2010, MNRAS 402, 836
Reis R.C., Miller J.M., 2013, ApJL 769, L7
Reis R.C., Miller J.M., Fabian A.C., et al., 2011, MNRAS 410, 2497
Remillard R.A., McClintock J.E., 2006, ARA&A 44, 49
Reynolds M.T., Miller J.M., Homan J., Miniutti G., 2010, ApJ 709, 358
Shidatsu M., Ueda Y., Tazaki F., et al., 2011, PASJ 63, 785
Steiner J.F., McClintock J.E., Remillard R.A., et al., 2010, ApJL 718, L117
Strüder L., Briel U., Dennerl K., et al., 2001, A&A 365, L18
Sunyaev R.A., Titarchuk L.G., 1980, A&A 86, 121
Tamura M., Kubota A., Yamada S., et al., 2012, ApJ 753, 65
Tomsick J.A., Corbel S., Kaaret P., 2001, ApJ 563, 229
Tomsick J.A., Kalemci E., Kaaret P., 2004, ApJ 601, 439

Tomsick J.A., Nowak M.A., Parker M., et al., 2014, ApJ 780, 78
Tomsick J.A., Yamaoka K., Corbel S., et al., 2009, ApJ 707, L87
Turner M.J.L., Abbey A., Arnaud M., et al., 2001, A&A 365, L27
Vargas M., Goldwurm A., Laurent P., et al., 1997, ApJL 476, L23
Verner D.A., Ferland G.J., Korista K.T., Yakovlev D.G., 1996, ApJ 465, 487
Wilkins D.R., Fabian A.C., 2012, MNRAS 424, 1284
Wilms J., Allen A., McCray R., 2000, ApJ 542, 914
Wu Q., Gu M., 2008, ApJ 682, 212
Yang Q.X., Xie F.G., Yuan F., et al., 2015, MNRAS 447, 1692
Zdziarski A.A., Johnson W.N., Magdziarz P., 1996, MNRAS 283, 193
Zdziarski A.A., Lubiński P., Smith D.A., 1999, MNRAS 303, L11
Życki P.T., Done C., Smith D.A., 1999, MNRAS 309, 561